Journal of
Synchrotron
Radiation

ISSN 0909-0495

Received 13 August 2010
Accepted 31 October 2010

Hard X-ray microbeam lithography using a Fresnel zone plate with a long focal length

S. Y. Lee,[a] I. H. Cho,[a] J. M. Kim,[a] H. C. Kang[b]* and D. Y. Noh[a]*

[a]School of Materials Science and Engineering, Gwangju Institute of Science and Technology, Gwangju 500-712, Korea, and [b]Department of Advanced Materials Engineering and BK21 Education Center of Mould Technology for Advanced Materials and Parts, Chosun University, Gwangju 501-759, Korea. E-mail: kanghc@chosun.ac.kr, dynoh@gist.ac.kr

Focused hard X-ray microbeams for use in X-ray nanolithography have been investigated. A 7.5 keV X-ray beam generated at an undulator was focused to about 3 μm using a Fresnel zone plate fabricated on silicon. The focused X-ray beam retains a high degree of collimation owing to the long focal length of the zone plate, which greatly facilitates hard X-ray nanoscale lithography. The focused X-ray microbeam was successfully utilized to fabricate patterns with features as small as 100 nm on a photoresist.

Keywords: hard X-ray focusing; Fresnel zone plate; X-ray lithography.

1. Introduction

As the scale of electronic devices approaches tens of nanometers, short-wavelength light sources are highly sought after for improving the pattern resolution of optical lithography (Suzuki & Smith, 2007). Although hard X-ray beams with wavelengths below 0.2 nm are optimal for nanolithography, the extremely weak interaction between X-rays and matter, as well as the absence of appropriate optical elements, has greatly limited their applications in lithography. Hard X-ray lithography is in its infancy at this stage and its resolution is far behind that of electron-beam lithography (Broers, 1995; Klymyshyn *et al.*, 2010). However, recent progress regarding optical elements for hard X-rays casts a chance to make improvements in hard X-ray lithography. Focusing X-rays to a small size is of great importance in X-ray microscopy and microprobes applicable to current nanobiotechnology that require an X-ray beam size comparable with the objects under probe with high brilliance (Diaz *et al.*, 2009; Chen, Wu *et al.*, 2008; Fukuda *et al.*, 2008; Vaschenko *et al.*, 2006; Paunesku *et al.*, 2009). In hard X-ray lithography, the increase in the photon flux by focusing facilitates overcoming the weak interaction of X-rays with photoresist (PR) materials, and reduces the exposure time substantially. During hard X-ray lithography, increasing photon flux by means of focusing discernibly helps to overcome the weak interaction between X-rays and PR, as well as substantially reducing exposure.

In order to focus X-rays within such small dimensions, researchers have extensively investigated various types of optical elements; for example, Kirkpatrick–Baez (KB) mirrors (Mimura *et al.*, 2007), multilayer Laue lenses (Kang *et al.*, 2006, 2008;), compound refractive lenses (Schroer *et al.*, 2005) and Fresnel zone plates (FZPs) (Chao *et al.*, 2005, 2009; Chen, Lo *et al.*, 2008; Vila-Comamala *et al.*, 2009). FZPs, representative diffractive optical elements, currently provide a spatial resolution of 15 nm in soft X-ray microscopy (Chao *et al.*, 2005) and 30 nm for hard X-ray microscopy at 8 keV (Chen, Lo *et al.*, 2008). FZPs are typically fabricated by means of electron-beam lithography and pattern transfer techniques. Notably, the FZP focusing capability can be improved by decreasing the outermost zone width and increasing the aspect ratio, *i.e.* the zone width to zone depth ratio (Kirz, 1974), since the focal spot size is proportional to the outermost zone width.

Different from microscopic applications of FZPs, which require the smallest possible focal spot, focusing efficiency and focused beam collimation are more relevant during hard X-ray lithography. To lithograph large repeated nanoscale features, the beam dimensions should be larger than a few micrometers. In addition, maintaining a high degree of collimation is required owing to the high penetration power of hard X-rays. To mask hard X-ray beams, a metal with a thickness >10 μm is required; the aspect ratio of the mask thickness to pattern features is more than 100 when the feature size decreases to the nanometer scale. Therefore, the angular divergence of an X-ray beam passing through a mask should be of the order of a few milliradians or less.

Since an X-ray beam of high flux is desirable in overcoming the weak interaction of hard X-rays during lithography, the focusing efficiency should be maximized. FZPs diffract hard X-rays weakly resulting in a relatively low focusing efficiency. The most effective FZPs currently available in hard X-ray microscopy have an aspect ratio of only 15 (Chen, Lo *et al.*, 2008), with a zone depth of less than 0.5 μm, and their efficiency remains at only a few percent (Maser *et al.*, 2004). Therefore, considerable effort has been exerted to fabricate hard X-ray FZPs with demonstrably higher efficiency. For example, researchers have designed deposition techniques to grow zone structures by sputtering (Kamijo *et al.*, 2003;

Tamura *et al.*, 2006) or chemical vapor deposition (Golant *et al.*, 2007; Artyukov *et al.*, 2009).

Recently, the European Synchrotron Radiation Facility group developed a process for fabricating FZPs by combining electron-beam and photo-lithography, deep plasma etching and anisotropic wet etching techniques (Snigireva *et al.*, 2007*a*). In contrast to conventional FZPs made on Si_3N_4 membranes, they fabricated FZPs on single-crystal Si wafers which provide excellent mechanical strength and thermal stability. Although Si is relatively transparent in the hard X-ray regime ($E \geq 7.5$ keV) compared with metals such as Au and Ni, patterned silicon zone structure provides sufficient phase shifts for focusing (Snigireva *et al.*, 2007*b*). Theoretical calculations indicate that the focusing efficiency of those FZPs at 7.5 keV is approximately 30%.

In this study we increased the X-ray photon flux by a factor of 300 by focusing a hard X-ray beam to about 3 µm using a Si-based FZP. The focused beam profile was recorded on a PR in a proximity lithography configuration. We successfully utilized the focused X-rays to produce patterns with a feature size as small as 100 nm on a PR using a specially fabricated hard X-ray mask based on multilayer growth techniques.

2. Focusing X-rays by a Si-based FZP

Fig. 1(*a*) shows an optical microscopy image of the FZP fabricated on silicon used in this study. The total number of zones N was 364; the outermost zone width Δr_n was 0.4 µm; the diameter D was 582 µm; and the zone depth was 9 µm. The aspect ratio, *i.e.* the ratio of the zone depth to Δr_n, was 22.5. The focal length f defined by $f = 4N(\Delta r_n)^2/\lambda$, where λ is the wavelength of X-rays and is proportional to the X-ray energy. For $\lambda = 1.65$ Å, f was approximately 1.412 m. Such a long focal length guaranteed the maximum angular divergence of the beam, D/f, to be $\sim 4 \times 10^{-4}$ rad.

A schematic diagram of the focusing geometry is illustrated in Fig. 1(*b*). The experiments were performed at undulator beamline 11A at the Pohang Light Source (PLS) in Korea. A liquid-nitrogen-cooled Si(111) double-crystal monochromator was used to select an X-ray energy of 7.5 keV ($\lambda = 1.65$ Å). The FZP was mounted on a motion stage to control the position and angle precisely. A pair of slits was installed upstream of the FZP to set the incident beam size to $\sim$600 µm in both horizontal and vertical directions. No central stop was used since the purpose of the focusing is to optimize X-ray flux rather than reducing focus size. A Ta pinhole with a diameter of 30 µm located 5 cm upstream of the primary focus was used as an order-sorting aperture (OSA), completely blocking higher-order diffraction signals allowing the exclusive use of the first-order focus. The focus size was estimated by scanning a micrometer-sized Ta pinhole across the primary focus.

Fig. 2(*a*) shows a line profile measured across the primary focus in the vertical direction. A Ta aperture with a diameter of 1 µm was scanned across the focused beam, intensity being monitored by a photodiode. The measured profile was fit to a single Gaussian profile displayed as a solid line in Fig. 2(*a*). The full width at half-maximum (FWHM) of the measured

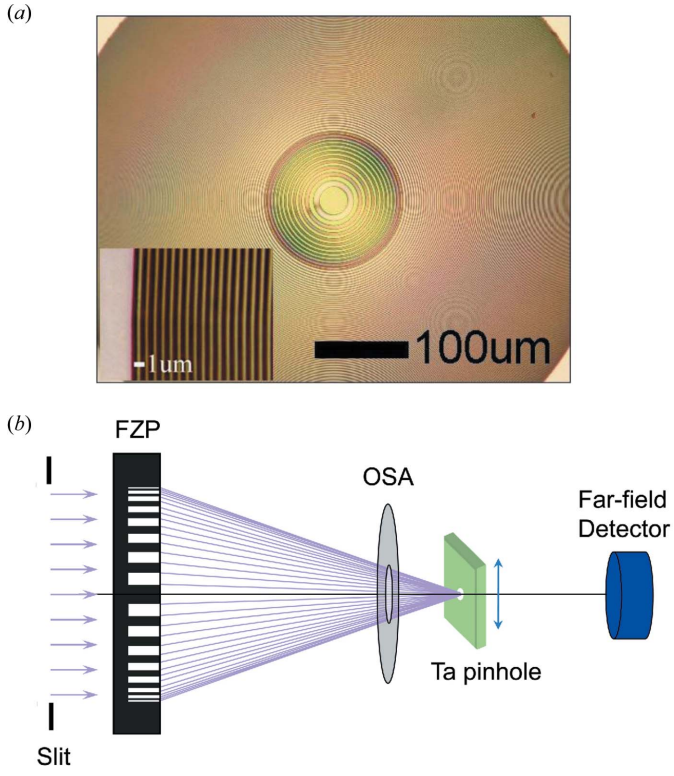

Figure 1
(*a*) Optical microscope image of the Fresnel zone plate fabricated on silicon used in this experiment. (*b*) Schematic drawing of the focusing geometry using the zone plate.

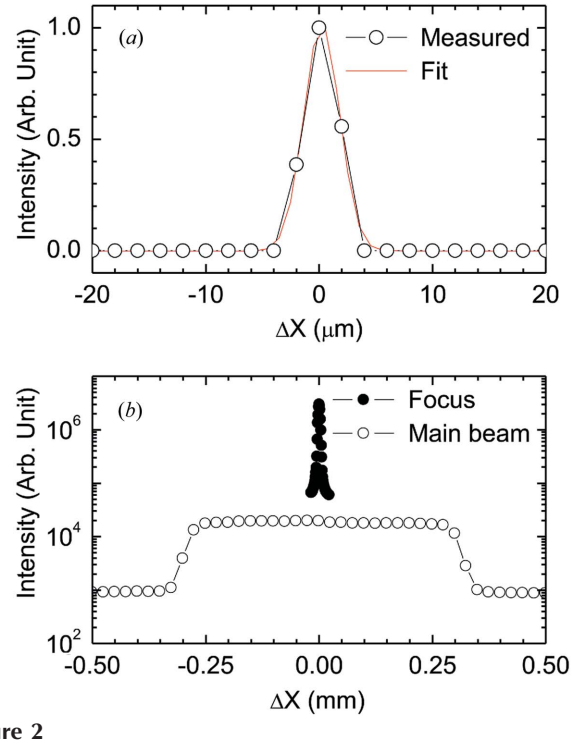

Figure 2
(*a*) Line profile of the focused beam in the vertical direction. A Gaussian fit was also shown. A FWHM of about 3 µm determines the size of the focus. (*b*) A comparison of the profile of the focused beam and direct main beam.

profile was approximately 3 μm, representing the focal spot size. The measured FWHM was much larger than the theoretical value of 0.5 μm set by the Rayleigh criterion, *i.e.* $R = 1.22\,\Delta r_n$ (Born & Wolf, 1980). This is attributed to the large source size and imperfect coherency of the incident beam. In addition, the finite size of the pinhole broadened the measured profile which is a convolution of the pinhole and the focused beam.

The focusing efficiency was estimated from the integrated intensity ratio between the focused beam and the unfocused direct beam. Fig. 2(*b*) shows their profiles. The unfocused beam profile revealed a rectangular shape in which the width represented the slit opening, whereas the focused beam was quite intense and sharp. Since FZPs are two-dimensional focusing optic elements, the X-ray intensities were integrated in both the vertical and horizontal directions. Based on the integrated intensity ratio, the focusing efficiency was estimated to be approximately 16%, which was higher than that of typical Au FZPs fabricated on Si_3N_4 membranes. Moreover, the efficiency might be further increased by increasing the zone depth. Among hard X-ray focusing devices, the efficiency of KB mirrors, about 50%, is considerably higher because they are based on the total external reflection. Alignment of the FZP, on the other hand, is relatively easier than aligning KB mirrors that require highly precise manipulators.

3. Results of focused hard X-ray beam lithography

First we recorded the focused X-ray beam and unfocused direct beam on a PR without placing any mask to evaluate the efficiency of the focusing and visually inspect the beam profile. ZEP520A-7 (Zeon, Japan), a high-performance positive PR typically used in electron-beam lithography, was employed. The PR was spin-coated on Si(001) substrates to a thickness of about 250 nm, which turned out to be the optimal thickness for features smaller than 500 nm. After exposure to X-rays, the PR was developed in a chemical developer (ZED-N50) and rinsed with isopropyl alcohol. The patterns were then examined by means of scanning electron microscopy (SEM). For SEM measurement, the samples were coated with a thin Pt layer for protection against high-energy electron beam as well as to minimize surface charging.

Fig. 3(*a*) shows an SEM image of the PR exposed by the unfocused direct beam. The direct beam shape defined by the silts with an opening size of 600 μm × 600 μm resulted in the square pattern. Figs. 3(*b*), 3(*c*) and 3(*d*) illustrate the focused beam replicated on the PR with exposure times of 4, 5 and 10 s, respectively. As shown in the figure, the patterning depends quite sensitively on the exposure time, suggesting that optimizing exposure time is critical for obtaining clear pattern formation.

Since hard X-ray lithography applications have been primarily limited by PR material sensitivity to hard X-rays, being much lower to electron beams, the most critical advantage of hard X-ray beam focusing in lithography is the X-ray photon flux. The exposure time required to produce the pattern shown in Fig. 3(*a*) by unfocused beam was as much as 50 min. Conversely, exposure was dramatically reduced to 5 s with the focused beam, indicating that the X-ray flux had increased over 300-fold owing to focusing.

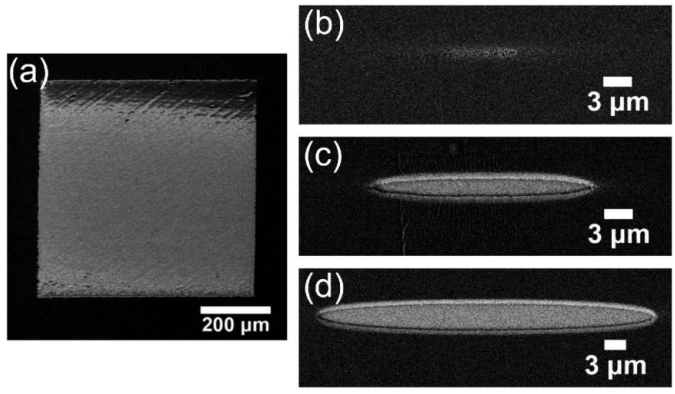

Figure 3
SEM images of the PR patterned by unfocused direct beam (*a*) and focused X-ray beam with exposure times of 4 s (*b*), 5 s (*c*) and 10 s (*d*), respectively.

Although the shape of the focused beam should be circular in principle, the PR recorded focused beam profile was elongated towards the horizontal direction as shown in Fig. 3(*c*), reflecting the anisotropic shape of the undulator source. The source size of the undulator beamline in PLS used in this experiment at 7.5 keV was approximately 200 μm and 20 μm in the horizontal and vertical directions, respectively. The source was demagnified at the focal plane (Vladimirsky *et al.*, 1999). In order to reduce the size in the horizontal direction at the focus, a slit was placed upstream of the beam, near the front-end of the beamline.

The focused X-ray microbeam shown in Fig. 3 was employed during the hard X-ray proximity lithography process in which a sectioned multilayer was used as a hard X-ray mask. The mask was prepared by alternately depositing a number of WSi_2 layers and Si layers and sectioning it in a direction perpendicular to the layers with a section depth of 20 μm. An SEM image of the mask thus prepared revealed that the thickness of the WSi_2 and Si layers was 310 nm and 380 nm, respectively, as shown in Fig. 4(*a*). The aspect ratio, *i.e.* the ratio of the transparent Si spacing to the section depth, was >60 and the X-rays have to travel through a long tunnel, requiring a highly collimated beam. As the feature size decreases to a few tens of nanometers, an even higher degree of collimation is necessary, which requires a focusing optic with a long focus similar to the one previously discussed. A detailed process of the mask preparation and the hard X-ray lithography conditions will be published elsewhere (Lee *et al.*, 2011). The focused X-ray beam was illuminated on the side of the multilayer section. The gap between the mask and the PR was controlled to optimize optical contrast. The hard X-ray lithography set-up is schematically illustrated in Fig. 4(*b*).

An SEM image of the pattern obtained by placing the multilayer mask at the focus is shown in Fig. 5(*a*). The gap between the mask and the PR was maintained at 200 μm, representing the optimal distance for clean patterning. Optimal exposure time was 40 s longer than the time used to

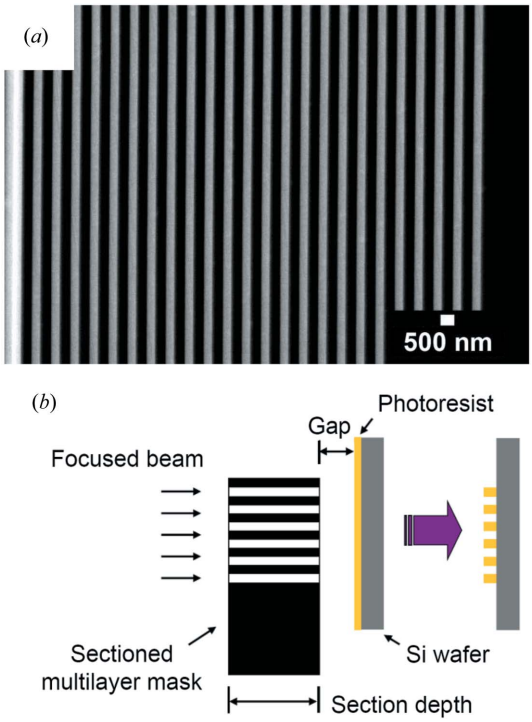

Figure 4
(*a*) SEM image of the sectioned multilayer mask with about 690 nm period. The white regions are opaque WSi_2 layers and the dark regions are transparent Si layers. (*b*) Schematic illustration of the hard X-ray proximity lithography set-up using the focused beam.

record the focused beam itself, which is attributable to the attenuation of the beam by the multilayer mask. A clear line-and-space pattern with sharp edges was observed. The line width at the center of the focused beam was about 300 nm and the period was about 690 nm. Such features are among the smallest in hard X-ray lithography reported up to now (Klymyshyn *et al.*, 2010). The lines (spaces) near the edge of the focused beam became thicker (thinner) indicating that the X-ray intensity weakened when approaching the edges. The size of the exposed area in the vertical direction is about 3 µm, corresponding to the size of the focused beam shown in Fig. 3(*c*).

One of the disadvantages of a focusing X-ray beam in lithography is that the total patterning area is limited by small beam size. As shown in Fig. 5(*a*), only a few lines can be fabricated with a focused beam. Patterning areas can be increased by either placing a mask and a PR away from the focus or rastering the focused beam, which is at the expense of the X-ray flux or exposure time. Fig. 5(*b*) shows an SEM image of a pattern obtained by placing the mask and the PR 50 mm downstream of the focus. Accordingly, beam size was increased to about 10 µm vertically and the number of patterned lines likewise increased significantly. Moreover, exposure also consistently increased by about a factor of five, while the patterning quality of the line-and-space structure remained similar to the one obtained at the focus. The exposure is believed to decrease to a few seconds using high-flux synchrotron sources, *i.e.* the Advanced Photon Source and

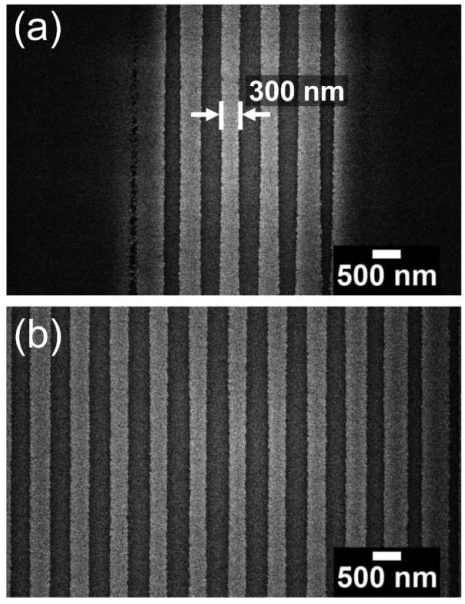

Figure 5
SEM image of the PR patterned by the hard X-ray beam at the focus position (*a*) and at 50 mm downstream of the focus position (*b*). The patterning area was enlarged away from the focus while the exposure time was increased.

SPring-8, which provide X-ray beams about a hundred times more intense than at PLS. The field of patterning area can also be increased by increasing the distance between the mask and the focus.

Finally, using the focused beam, we tested a mask with a reduced feature size to determine the patterning resolution limit. A mask fabricated using a multilayer with 200 nm-thick WSi_2 layers and 100 nm-thick Si layers was placed at the focus position. Fig. 6 shows an SEM image of the pattern recorded on the PR using such a mask. The width of the thinnest line, shown in the inset of the figure, measured about 100 nm with the line edge roughness near 20 nm. The lines in the central region, where the beam is more intense, narrowed slightly. We note that the morphology of the PR remaining in the lines was not uniform but exhibited local agglomerations needing to be suppressed in order to improve the pattern resolution below 100 nm. In order to reduce the pattern resolution towards the 10 nm scale, the interaction mechanism between hard X-rays and the PR should be investigated more closely. According to our simulation of the wavefield inside and downstream of the multilayer mask, it was obvious that contrast in the X-ray beam is high enough to be patterned on PR even when the mask feature size is scaled down to 10 nm. By employing two crossed multilayer masks, periodic dot patterns can be achieved. Nevertheless, patterns with arbitrary shape are limited when employing the multilayer as a mask.

4. Conclusion

In summary, we characterized the focusing properties of a Si-based FZP with a focal length of about 1.4 m. In particular, we obtained a micrometer-sized X-ray focus and applied it to

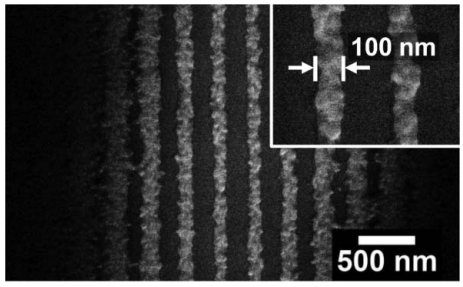

Figure 6
Pattern fabricated with a WSi_2(200 nm)–Si(100 nm) mask. The inset shows the line at the center whose thickness is about 100 nm.

hard X-ray lithography. We have fabricated lines with a width of about 300 nm, and demonstrated a capability to fabricate 100 nm-thick lines. With a high focusing efficiency, the exposure time to pattern the PR was reduced significantly, even though the focusing was not completely optimized. Moreover, with continuous improvements in hard X-ray sources and PR, the hard X-ray lithography demonstrated in this study can be extended to a nanometer-scale resolution lithography. Intense X-ray microbeam with an excellent degree of collimation can also be applied to high-resolution X-ray microbeam diffraction experiments in which the X-ray beam size is similar to that of the samples.

We thank S. N. Kim and Chan Kim for their help in the experimental set-up. This research was supported by the National Research Foundation of Korea (NRF) through the NCRC (R15-2008-006-01000-0), WCU (R31-2008-000-10026-0), general user program (No. 2010-0023604) and GIST Top Brand grants. This work was also supported by a grant (code 20090006) from Development of Marine Environmental Sensor using Nano and Photonics Technology Project funded by the Ministry of Maritime Affairs and Fisheries of the Korean government.

References

Artyukov, I. A., Bukreeva, I. N., Chernov, V. A., Reshchenko, R. M., Golant, K. M., Jark, W., Lavrishchev, S. V., Mitrofanov, A. N., Popov, A. V. & Vinogradov, A. V. (2009). *Nucl. Instrum. Methods Phys. Res. A*, **603**, 66–68.

Born, M. & Wolf, E. (1980). *Principles of Optics*, 6th ed. New York: Pergamon.

Broers, A. N. (1995). *Philos. Trans. R. Soc. London Ser. A*, **353**, 291.

Chao, W. L., Harteneck, B. D., Liddle, J. A., Anderson, E. H. & Attwood, D. T. (2005). *Nature (London)*, **435**, 1210–1213.

Chao, W. L., Kim, J., Rekawa, S., Fischer, P. & Anderson, E. H. (2009). *Opt. Express*, **17**, 17669–17677.

Chen, J., Wu, C., Tian, J., Li, W., Yu, S. & Tian, Y. (2008). *Appl. Phys. Lett.* **92**, 233104.

Chen, Y. T., Lo, T. N., Chu, Y. S., Yi, J., Liu, C. J., Wang, J. Y., Wang, C. L., Chiu, C. W., Hua, T. E., Hwu, Y., Shen, Q., Yin, G. C., Liang, K. S., Lin, H. M., Je, J. H. & Margaritondo, G. (2008). *Nanotechnology*, **19**, 395302.

Diaz, A., Mocuta, C., Stangl, J., Mandl, B., David, C., Vila-Comammala, J., Chamard, V., Metzger, T. H. & Bauer, G. (2009). *Phys. Rev. B*, **79**, 125324.

Fukuda, N., Hokura, A., Kitajima, N., Terada, Y., Saito, H., Abe, T. & Nakai, I. (2008). *J. Anal. At. Spectrom.* **23**, 1068–1075.

Golant, K. M., Lavrishchev, S. V., Popov, A. V., Artyukov, I. A., Feshchenko, R. M., Mitrofanov, A. N. & Vinogradov, A. V. (2007). *Appl. Opt.* **46**, 5964–5966.

Mimura, H., Yumoto, H., Matsuyama, S., Sano, Y., Yamamura, K., Mori, Y., Yabashi, M., Nishino, Y., Tamasaku, K., Ishikawa, T. & Yamauchi, K. (2007). *Appl. Phys. Lett.* **90**, 051903.

Kamijo, N., Suzuki, Y., Takano, H., Tamura, S., Yasumoto, M., Takeuchi, A. & Awaji, M. (2003). *Rev. Sci. Instrum.* **74**, 5101–5104.

Kang, H. C., Maser, J., Stephenson, G. B., Liu, C., Conley, R., Macrander, A. T. & Vogt, S. (2006). *Phys. Rev. Lett.* **96**, 127401.

Kang, H. C., Yan, H., Winarski, R. P., Holt, M. V., Maser, J., Liu, C., Conley, R., Vogt, S., Macrander, A. T. & Stephenson, G. B. (2008). *Appl. Phys. Lett.* **92**, 221114.

Kirz, J. (1974). *J. Opt. Soc. Am.* **64**, 301–309.

Klymyshyn, D. M., Mappes, T., Achenbach, S., Kachayev, A., Borner, M. & Mohr, J. (2010). *J. Micromech. Microeng.* **20**, 075031.

Lee, S. Y., Cho, I. H., Kim, J. M., Yan, H., Conley, R., Liu, C., Macrander, A. T., Maser, J., Stephenson, G. B., Kang, H. C. & Noh, D. Y. (2011). In preparation.

Maser, J., Stephenson, G. B., Vogt, S., Yun, W., Macrander, A. T., Kang, H. C., Liu, C. & Conley, R. (2004). *Proc. SPIE*, **5539**, 185–194.

Paunesku, T., Vogt, S., Irving, T. C., Lai, B., Barrea, R. A., Maser, J. & Woloschak, G. E. (2009). *Int. J. Radiat. Biol.* **85**, 710–713.

Schroer, C. G., Kurapova, O., Patommel, J., Boye, P., Feldkamp, J., Lengeler, B., Burghammer, M., Riekel, C., Vincze, L., van der Hart, A. & Kuchler, M. (2005). *Appl. Phys. Lett.* **87**, 124103.

Snigireva, I., Snigirev, A., Kohn, V., Yunkin, V., Grigoriev, M., Kuznetsov, S., Vaughan, G. & Michiel, M. D. (2007*a*). *Phys. Status Solidi A*, **204**, 2817–2823.

Snigireva, I., Snigirev, A., Kohn, V., Yunkin, V., Grigoriev, M., Kuznetsov, S., Vaughan, G. & Michiel, M. D. (2007*b*). *Proc. SPIE*, **6705**, 67050G.

Suzuki, K. & Smith, B. W. (2007). *Microlithography: Science and Technology*, 2nd ed. Boca Raton: CRC.

Tamura, S., Yasumoto, M., Kamijo, N., Suzuki, Y., Awaji, M., Takeuchi, A., Uesugi, K., Terada, Y. & Takano, H. (2006). *Vacuum*, **80**, 823–827.

Vaschenko, G., Brewer, C., Brizuela, F., Wang, Y., Larotonda, M. A., Luther, B. M., Marconi, M. C., Rocca, J. J., Menoni, C. S., Anderson, E. H., Chao, W., Harteneck, B. D., Liddle, J. A., Liu, Y. & Attwood, D. T. (2006). *Opt. Lett.* **31**, 1214–1216.

Vila-Comamala, J., Jefimovs, K., Raabe, J., Pilvi, T., Fink, R. H., Seonner, M., Maabdorf, A. Ritala, M. & David, C. (2009). *Ultramicroscopy*, **109**, 1360–1364.

Vladimirsky, Y., Bourdilon, A., Vladimirsky, O., Jiang, W. & Leonard, Q. (1999). *J. Phys. D*, **32**, L114–L118.